

A. B. Bonds, *Vis. Neurosci.* **6**, 239 (1991); I. Ohzawa, G. Sclar, R. D. Freeman, *J. Neurophysiol.* **54**, 651 (1985); P. Lennie, M. J. M. Lankheet, J. Krauskopf, *Invest. Ophthalmol. Vis. Sci. (suppl.)* **35**, 1662 (1994).

9. I. Ohzawa, G. Sclar, R. D. Freeman, *J. Neurophysiol.* **54**, 651 (1985); W. S. Geisler and D. G. Albrecht, *Vision Res.* **32**, 1409 (1992); D. J. Heeger, *Vis. Neurosci.* **9**, 181 (1992); M. Carandini, D. J. Heeger, J. A. Movshon, *J. Neurosci.* **17**, 8621 (1997).

10. W. S. Geisler and D. G. Albrecht, *Vision Res.* **32**, 1409 (1992).

11. A. B. Bonds, *Vis. Neurosci.* **6**, 239 (1991); D. J. Heeger, *Ibid* **9**, 181 (1992); G. C. DeAngelis, J. G. Robson, I. Ohzawa, R. D. Freeman, *J. Neurophysiol.* **68**, 144 (1992).

12. J. A. Movshon and P. Lennie, *Nature* **278**, 850 (1979); A. B. Saul and M. S. Cynader, *Vis. Neurosci.* **2**, 593 (1989); *ibid.*, p. 609; M. Carandini, H. B. Barlow, L. P. O'Keefe, A. B. Poirson, J. A. Movshon, *Philos. Trans. R. Soc. London Ser. B* **352**, 1149 (1997).

13. H. B. Barlow, D. I. A. MacLeod, A. van Meeteren, *Vision Res.* **16**, 1043 (1976); D. Regan and K. I. Beverley, *J. Opt. Soc. Am.* **2**, 147 (1985); M. W. Greenlee and F. Heitger, *Vision Res.* **28**, 791 (1988).

14. At the beginning of each trial lasting 1.75 s, an adapting grating (or a blank field) was presented for 0.5 s. This was followed after 215 ms (Fig. 2A) or 27 ms (Fig. 2B) by a 94-ms presentation of a test grating at one of 10 orientations ( $0^\circ, \pm 7^\circ, \pm 14^\circ, \pm 21^\circ, \pm 28^\circ, \text{ or } +90^\circ$ ), or by nothing. Discharge rate was calculated from the whole response to the test grating. Gratings had optimal spatial frequency, size, and position, and 100% contrast. In successive trials the different adapting and test grating pairs were randomly interleaved, and each such trial was repeated 40 times. When no grating was visible, the screen displayed a spatially uniform field of the average luminance.

15. Orientation tuning before adaptation was similar whether measured with stationary or moving gratings. Orientation tuning before and after adaptation was summarized by the center-of-mass  $\sum iR_i$  of the responses to stimuli with orientations  $i \in \{0^\circ, \pm 7^\circ, \pm 14^\circ, \pm 21^\circ, \pm 28^\circ\}$ . For sharply (and symmetrically) tuned neurons with half-width  $< 28^\circ$  this is exactly the preferred orientation. For all neurons it increases monotonically with preferred orientation. The average neuron's center-of-mass changed by  $1.5^\circ$ .

16. To estimate the discriminability of two gratings we measured a series of responses to each, and for the resulting distributions of response amplitudes computed the means  $\pm$  SDs. We treated the distributions as normal and calculated the difference between their means divided by the root-mean-square standard deviation  $d' = \frac{\mu_1 - \mu_2}{\sqrt{(\sigma_1^2 + \sigma_2^2)/2}}$  [D. M. Green and J. A. Swets,

$$\psi(\theta) = \frac{\sum_{\text{All cells}} \text{Resp}(\text{cell A}, \theta) \cdot \text{Resp}(\text{cell B}, \theta)}{\text{Number of cell pairs}}$$

the average, unnormalized, point-by-point product of the responses of all pairs of neurons. This is an

intermediate stage in the calculation of the cross-correlation. To establish how adaptation reduces the redundancy among responses, we calculate  $\psi$  before and after adaptation, for probes at a range of orientations. We treat every neuron as if it had been adapted to the pattern at orientation  $0^\circ$ .

20. E. P. Simoncelli and O. Schwartz, in *Advances in Neural Information Processing Systems 11*, M. S. Kearns, S. A. Solla, D. A. Cohn, Eds. (MIT Press, Cambridge, MA, 1999).

21. L. Maffei and A. Fiorentini, *Vision Res.* **16**, 1131 (1976); J. I. Nelson and B. J. Frost, *Brain Res.* **139**, 359 (1978); G. C. DeAngelis, R. D. Freeman, I. Ohzawa, *J. Neurophysiol.* **71**, 347 (1994); A. M. Sillito, K. L. Grieve, H. E. Jones, J. Cudeiro, J. Davis, *Nature* **378**, 492 (1995); J. B. Levitt and J. S. Lund, *ibid.* **387**, 73 (1997).

22. Sharpened orientation selectivity has been suggested [J. I. Nelson and B. J. Frost, *Brain Res.* **139**, 359 (1978); C. Blakemore and E. A. Tobin, *Exp. Brain Res.* **15**, 439 (1972)] and is among the constellation of changes in orientation selectivity reported by Gilbert and Wiesel [C. D. Gilbert and T. N. Wiesel, *Vision Res.* **30**, 1689 (1990)].

23. L. Maffei and A. Fiorentini [*Vision Res.* **16**, 1131 (1976)] suggested that adaptation sharpens spatial frequency tuning.

24. See, for example, A. T. Bahill, D. Adler, L. Stark, *Invest. Ophthalmol.* **14**, 468 (1975). The distribution of saccade sizes is heavily task-dependent [for example, M. F. Land and S. Furneaux, *Philos. Trans. R. Soc. London Ser. B* **352**, 1231 (1997)].

25. M. Carandini and D. Ferster, *Science* **276**, 949 (1997).

26. M. Carandini, personal communication.

27. H. Markram and M. Tsodyks, *Nature* **382**, 807 (1996); F. S. Chance, S. B. Nelson, L. F. Abbott, *J. Neurosci.* **18**, 4785 (1998); L. F. Abbott, J. A. Varela, K. Sen, S. B. Nelson, *Science* **275**, 220 (1997).

28. A surrounding grating brought about significant changes in orientation tuning in almost half of the complex cells we studied.

29. All animal procedures were approved by the University of Rochester committee for the care and use of laboratory animals. Funded by NIH grants EY04440, EY01319, EY06638, and EY07125.

3 May 1999; accepted 26 July 1999

## Altered Cochlear Fibrocytes in a Mouse Model of DFN3 Nonsyndromic Deafness

O. Minowa,<sup>1,3\*</sup> K. Ikeda,<sup>2\*</sup> Y. Sugitani,<sup>1,3</sup> T. Oshima,<sup>2</sup> S. Nakai,<sup>1,3</sup> Y. Katori,<sup>2</sup> M. Suzuki,<sup>2</sup> M. Furukawa,<sup>2</sup> T. Kawase,<sup>2</sup> Y. Zheng,<sup>2</sup> M. Ogura,<sup>2</sup> Y. Asada,<sup>2</sup> K. Watanabe,<sup>2</sup> H. Yamanaka,<sup>1,3</sup> S. Gotoh,<sup>1,2</sup> M. Nishi-Takeshima,<sup>5</sup> T. Sugimoto,<sup>6</sup> T. Kikuchi,<sup>2</sup> T. Takasaka,<sup>2</sup> T. Noda<sup>1,3,4,†</sup>

DFN3, an X chromosome-linked nonsyndromic mixed deafness, is caused by mutations in the *BRN-4* gene, which encodes a POU transcription factor. *Brn-4*-deficient mice were created and found to exhibit profound deafness. No gross morphological changes were observed in the conductive ossicles or cochlea, although there was a dramatic reduction in endocochlear potential. Electron microscopy revealed severe ultrastructural alterations in cochlear spiral ligament fibrocytes. The findings suggest that these fibrocytes, which are mesenchymal in origin and for which a role in potassium ion homeostasis has been postulated, may play a critical role in auditory function.

Hereditary deafness affects about 1 in 2000 children and 70% of the cases occur nonsyndromically (in the absence of other associated clinical features). DFN3, an X chromosome-linked nonsyndromic deafness, is clinically

characterized by a conductive hearing loss, a flow of perilymph during the opening of the stapes footplate, and progressive sensorineural deafness (1). Genetic studies have shown that DFN3 is caused by mutations in *BRN-4/RHS2/POU3F4*, which encodes a POU transcription factor (2). The role of *Brn-4* in the development of auditory function, however, remains unclear. Mutations in *BRN-3.1/BRN-3c*, which encodes another POU factor, are responsible for hereditary nonsyndromic deafness, DFNA15, and targeted mutagenesis in mice has suggested that the protein plays a critical role in differentiation of hair cells in the inner ear (3). During development, *Brn-4* is expressed throughout the inner ear in the mesenchyme of both the cochlear and vestibular aspects but not in tissues derived from neuroepithelial or neuronal cells (4).

To analyze *Brn-4* function in vivo and to elucidate possible mechanisms underlying DFN3, we generated *Brn-4*-deficient mice by

<sup>1</sup>Department of Cell Biology, The Cancer Institute, Japanese Foundation for Cancer Research, 1-37-1 Kami-ikebukuro, Toshima-ku, Tokyo 170-8455, Japan. <sup>2</sup>Department of Otorhinolaryngology, Tohoku University School of Medicine, 1-1 Seiryō-machi, Aoba-ku, Sendai 980-8574, Japan. <sup>3</sup>CREST, Japan Science and Technology Corporation, 4-1-8 Motomachi, Kawaguchi 332-0012, Japan. <sup>4</sup>Department of Molecular Genetics, Tohoku University School of Medicine, 2-1 Seiryō-machi, Aoba-ku Sendai 980-8575, Japan. <sup>5</sup>Department of Pharmacology, Faculty of Medicine, University of Tokyo, 7-3-1 Hongo, Bunkyo-ku, Tokyo 113-8655, Japan. <sup>6</sup>Department of Anatomy, Kansai Medical University, 10-15 Fumizono-cho, Moriguchi-shi, Osaka 570-8506, Japan.

\*These authors contributed equally to this work.

†To whom correspondence should be addressed. E-mail: tnoda@ims.u-tokyo.ac.jp

## REPORTS

targeted mutagenesis. A targeting vector was constructed that enabled us to replace a 2-kb genomic sequence containing the entire coding region of *Brn-4* with a pgk-neo (neomycin-resistance gene driven by phosphoglycerate kinase gene promoter) cassette (Fig. 1A) (5). Homologous recombination was confirmed in 1 of 330 G418-resistant embryonic stem (ES) cell clones (Fig. 1B). This clone was injected into blastocysts from C57BL/6 mice and the resulting chimeras were mated to C57BL/6 mice. Germ line transmission of the mutant *Brn-4* allele was confirmed by Southern blotting. Mating of heterozygous F<sub>1</sub> females with male chimeras yielded homozygous males and females. Gel mobility-shift assays (6) indicated that the homozygous mutants had no DNA binding activity attributable to Brn-4 (Fig. 1C). Mice deficient for

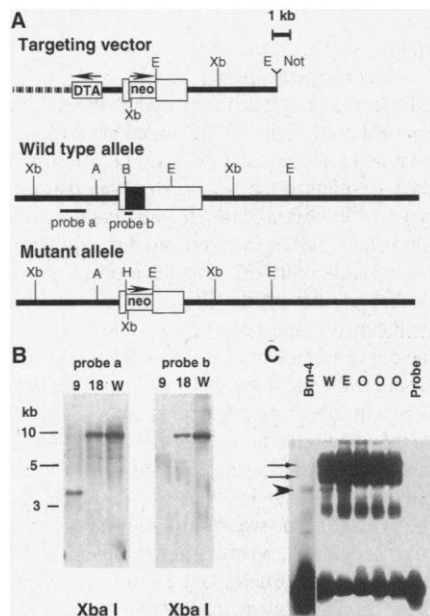


**Fig. 1.** Targeted inactivation of the *Brn-4* gene. (A) Diagram of the targeting vector and wild-type and mutant alleles. *Brn-4* open reading frame is indicated by the black box; exon is indicated by the open box. neo, neomycin-resistance gene driven by phosphoglycerate kinase gene promoter (pgk-neo); DTA, diphtheria toxin A-chain gene; A, Acc I; E, Eco RI; H, Hind III; B, Bam HI; Xb, Xba I. (B) Southern blot analysis of recombinant (#9), randomly integrated (#18), and wild-type (W) ES cell clones by Xba I digestion. Map locations of probes a and b are shown in (A). The mutant allele was detected as a 4.4-kb fragment. Homologous recombinant ES clone (#9) shows only the mutant allele band because mouse *Brn-4* is located on the X chromosome. (C) DNA binding activity of Brn-4 protein in brain extracts at postnatal day 0 from wild-type male (W), heterozygous female (E), and homozygous mutant female (O) mice, analyzed by gel-shift assay. An extract of *Brn-4*-transfected NIH 3T3 cells and an assay mix without cell extract (probe) were used as controls. Arrowhead indicates band shifted by Brn-4 binding. Arrows indicate bandshifts caused by Brn-1 (upper) and Brn-2 (lower).

*Brn-4* appeared to be normal and were fertile.

To assess the auditory function of *Brn-4*-deficient mice, we measured the auditory brainstem response (ABR) (7). Wild-type male mice showed a typical ABR waveform and waves I to V were clearly identified above the 30-decibel (dB) sound pressure level (SPL). In contrast, *Brn-4* mutant male mice showed an ABR response only with stimuli above a 90-dB SPL (Fig. 2A). At 11 weeks of age, the average ABR threshold in wild-type mice was 23-dB SPL for males and 25-dB SPL for females,

whereas the average in *Brn-4*-deficient mice was 89-dB SPL for males and 92-dB SPL for homozygous females, which is indicative of profound deafness (Fig. 2B). The ABR consisted of multiple waves, corresponding to successive activation of nuclei transmitting neural signals from the periphery to the central region. Thus, the lack of wave I at 30- to 70-dB SPL in mutant mice suggested that the cause of deafness resided in neurons of the spiral ganglion or more peripheral regions, including the cochlea and conductive apparatus. *Brn-4*-deficient mice

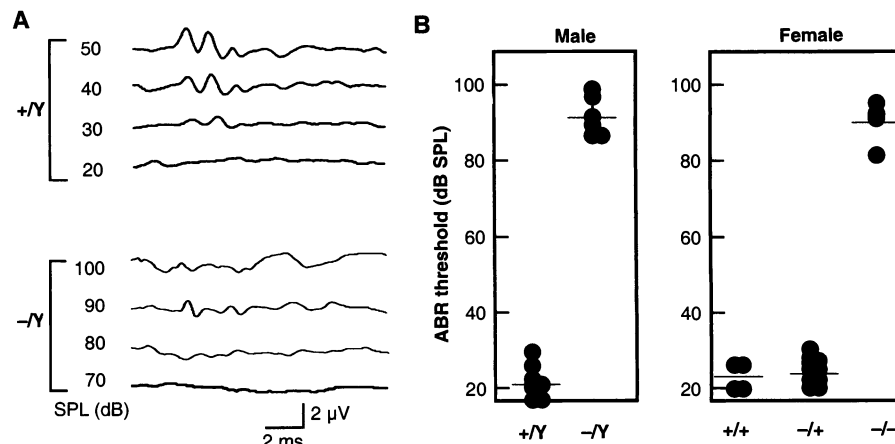


**Fig. 2.** ABRs of wild-type and *Brn-4*-deficient mice. (A) ABR waveforms of wild-type (+/Y) and *Brn-4* mutant (-/Y) males at 11 weeks of age, measured at 20- to 50-dB SPL and 70- to 100-dB SPL, respectively. (B) Scatterplots of ABR thresholds for 11-week-old male and female mice. Horizontal bars denote averages for each group. +/Y and +/+, wild type; -/+, heterozygote; -/Y and -/-, *Brn-4*-deficient mice.

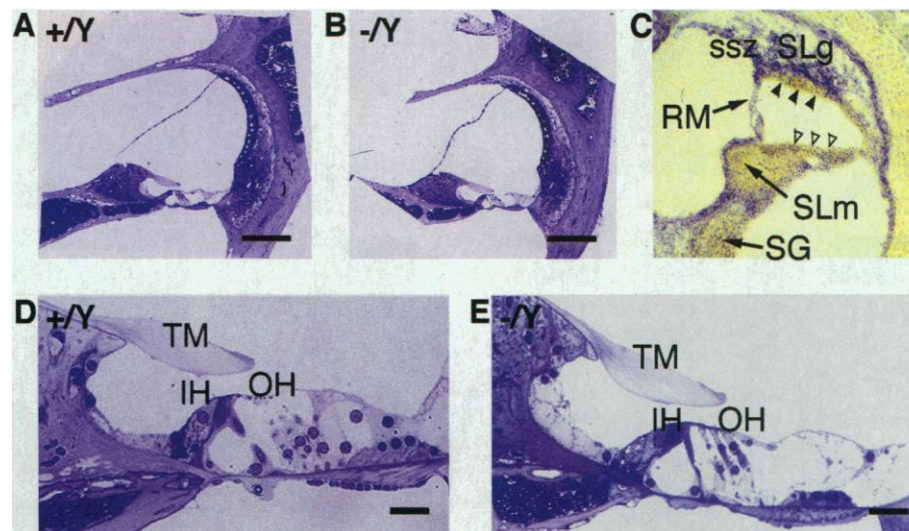


**Fig. 3.** Histological analysis of the cochlear duct of *Brn-4* mutants and expression of *Brn-4* in the cochlear duct of mice. (A) Morphology of the basal turn of the cochlea of an 11-week-old wild-type male. (B) Basal turn of the cochlea of an 11-week-old *Brn-4* mutant male. Scale bars = 100  $\mu$ m. (C) In situ hybridization analysis of *Brn-4* mRNA expression. Cochlear section of a wild-type female at postnatal day 0 is shown. *Brn-4* mRNA expression is evident as a blue precipitate. The following structures are indicated: spiral ligament (SLg), suprastrial zone (ssz), Reissner's membrane (RM), stria vascularis (filled arrowheads), organ of Corti (open arrowheads), spiral limbus (SLm), spiral ganglion (SG). (D and E) Images at higher magnification showing the organ of Corti of a wild-type male (D) and a *Brn-4* mutant male (E). IH, inner hair cells; OH, outer hair cells; TM, tectorial membrane. Scale bars = 10  $\mu$ m.

## REPORTS

could swim normally, which indicates that they had a normal vestibular function.

To determine whether the mutant mice had an impaired conductive apparatus, we examined the middle ear structure of 11-week-old males under a dissecting microscope. The structures of the tympanic membrane and an ossicular chain—consisting of malleus, incus, and stapes—appeared to be normal in mutant mice. Intact structures were confirmed by histological analysis (8). Although human DFN3 patients showed stapes fixation (1), the flexibility of auditory ossicle junctions and the mobility of stapes footplates of the mutant mice were indistinguishable from those of wild-type mice.

The absence of gross defects in the middle ear organs suggested that the primary lesion resided in the inner ear cochlear system or in the auditory nerves. Analysis of the inner ear structures of 11-week-old *Brn-4*-deficient male mice by light microscopy (9) revealed the normal appearance of the cochlear duct, including the organ of Corti, the spiral ganglion, and the stria vascularis (Fig. 3, A and B). The organ of Corti had a well-differentiated structure consisting of inner and outer hair cells and several types of supporting cells, including pillar cells and Deiters' cells resting on the basilar membrane (Fig. 3, D and E). The tectorial membrane

was also normal in the mutant mice. Thus, although *Brn-4* is highly expressed in the developing inner ear (4), we detected no gross abnormality of the inner ear in the *Brn-4*-deficient mice.

We next analyzed *Brn-4* mRNA expression in the inner ears of wild-type neonatal mice by *in situ* hybridization (10) (Fig. 3C). The highest level of expression was detected in the spiral ligament, a connective tissue structure containing three types of fibrocytes (types 1, 2, and 3) (11) as predominant cellular components. Type 1 fibrocytes occupy the region beneath the stria vascularis. Type 2 fibrocytes are found in the suprastrial zone and the central area of the spiral ligament beneath the spiral prominence. Type 3 fibrocytes form a cell layer attached to the otic capsule. Our results suggested that all three fibrocyte types expressed *Brn-4*. Reissner's membrane, the edge of the spiral limbus, and the region between the spiral limbus and the spiral ganglion also contained *Brn-4* mRNA but in lower amounts than the spiral ligament. The organ of Corti (including the inner and outer hair cells), the stria vascularis, the spiral limbus, and the spiral ganglion were negative for *Brn-4*, which suggests that *Brn-4* expression is limited to cells of mesodermal origin.

Analysis of fibrocyte ultrastructure by trans-

mission electron microscopy (TEM) (12) revealed remarkable pathological changes in the spiral ligament fibrocytes in all turns of the cochlea of 11-week-old *Brn-4*-deficient mice. In wild-type mice, type 2 fibrocytes in the suprastrial zone had a highly convoluted shape with numerous cytoplasmic extensions (Fig. 4, A and B) and showed an abundance of mitochondria (Fig. 4B). In mutant mice, these fibrocytes had markedly fewer cytoplasmic extensions and both the volume of cytoplasm and the number of mitochondria were dramatically reduced (Fig. 4, E and F). Type 1 fibrocytes filling the area beneath the stria vascularis also had few mitochondria (Fig. 4G) and the surrounding extracellular matrix was extremely sparse compared with wild-type mice (Fig. 4C). Further analysis of *Brn-4* mutants by transmission and scanning electron microscopy revealed no pathological features in other structures of the inner ear, including inner and outer hair cells (Fig. 4, D and H), the stria vascularis, the spiral ganglia, and the auditory nerve (13).

According to a recent hypothesis (11), type 2 fibrocytes may take up perilymphatic  $K^+$  ions by means of their  $Na^+, K^+$ -adenosine triphosphatase (ATPase) activity. These  $K^+$  ions may then be transported to the stria vascularis by type 1 fibrocytes through gap junctions and ultimately may be secreted into the endolymph; this would contribute to generation of the endocochlear potential (EP), a resting potential maintained in the extracellular fluid that bathes the upper surface of mechanosensory hair cells. Because the pathological findings in the spiral ligament fibrocytes described above strongly suggested fibrocyte dysfunction in *Brn-4*-deficient mice, we measured EP values in the mutant mice (14). In 11-week-old wild-type mice the average value was 85 mV for males and 91 mV for females, whereas in the mutants it was only 38 mV for males and 39 mV for females (Fig. 5). This mutant phenotype suggests that *Brn-4* plays a critical role in the generation or maintenance of the EP by controlling development of fibrocytes along the cochlear duct. Any

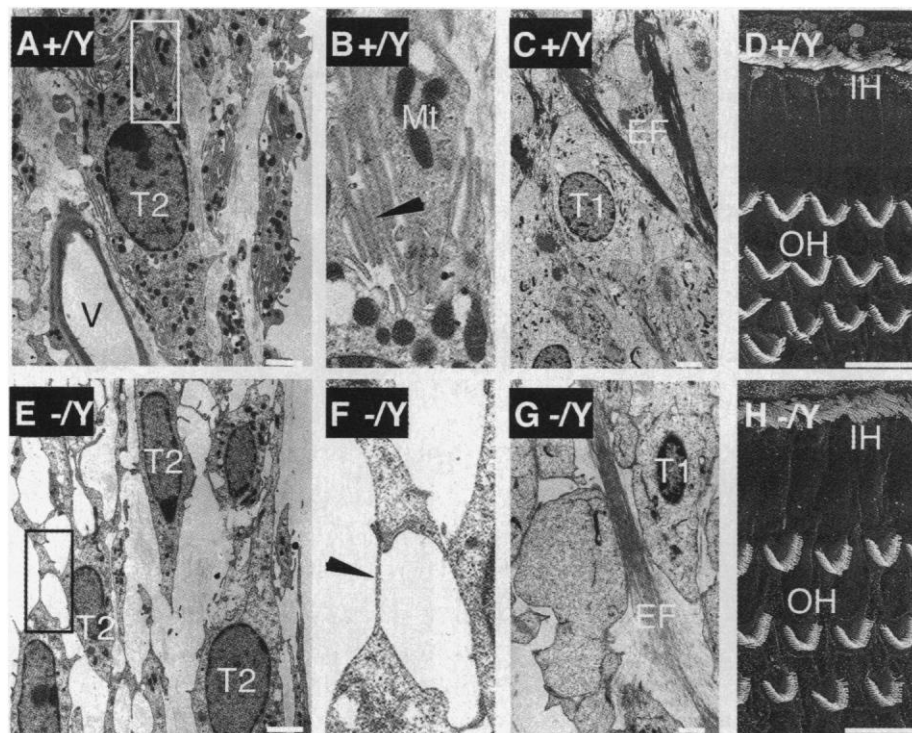


**Fig. 4.** Electron microscopic features of the cochlear duct of *Brn-4* mutants ( $-/Y$ ) (E–H) and wild-type mice ( $+/Y$ ) (A–D) at 11 weeks of age. (A and E) TEM analysis of the suprastrial zone of the spiral ligament. T2, type 2 fibrocyte. Scale bars = 2  $\mu$ m. (B and F) Magnification of rectangular regions in (A) and (E), respectively. Arrowheads indicate plasma membrane projections. Note the dramatic difference in cell shape and the reduced number of mitochondria (Mt) in the mutant. (C and G) TEM analysis of fibrocytes behind the stria vascularis. T1, type 1 fibrocyte; EF, extracellular filament. Scale bars = 2  $\mu$ m. (D and H) Scanning electron microscopy of hair cell stereocilia, showing normal shape and arrangement in both *Brn-4* mutant and wild-type mice. IH, inner hair cell; OH, outer hair cell. Scale bars = 10  $\mu$ m.

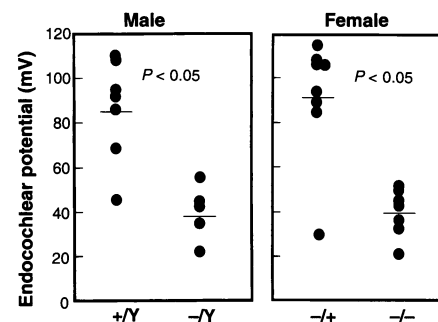


**Fig. 5.** Decreased EP in *Brn-4*-deficient males and females at 11 weeks of age.  $-/Y$ , male mutant;  $+/Y$ , male wild-type control;  $-/-$ , female mutant;  $-/+$ , female heterozygote control. Horizontal bars denote averages for each group of mice.

abnormality of fibrocytes in the spiral ligament would be expected to disrupt K<sup>+</sup> transport, leading to depression of the EP. A reduced EP would explain the elevation of ABR thresholds in mutants as the receptor potential of hair cells depends on the magnitude of the EP (15). The idea that fibrocytes contribute to the generation or maintenance of the EP is thus strongly supported by our present finding.

In the past 5 years, 13 human genes have been identified that are responsible for hereditary nonsyndromic deafness (16). Mouse models harboring mutations in the homologous genes are available for *Brn 3.1/Brn-3c* and for the myosin VIIA (shaker 1) and myosin XV (shaker 2) genes. In all three of these models, the mice suffer sensorineural deafness because of defects in sensory hair cells of the inner ear. Our analysis of *Brn-4*-deficient mice has indicated that cochlear fibrocytes, which are non-sensory mesenchymal cells specific to the cochlear duct, may also play an important role in auditory function. Given the high level of *Brn-4* expression in fibrocytes, the pathological changes may be a cell autonomous consequence of *Brn-4* deficiency, as is the case for other members of the POU transcription factor family (17). Because the number of fibrocytes in *Brn-4*-deficient mice is similar to that in wild-type mice (9), *Brn-4* may be essential for the differentiation or function of fibrocytes but not for their survival. The fibrocytes are rich in Na<sup>+</sup>,K<sup>+</sup>-ATPase and the gap junction protein connexin 26 (11), which are thought to be essential for K<sup>+</sup> transport, and mutations in the *GJB2* gene encoding connexin 26 have been shown to be responsible for DFNB1, another nonsyndromic deafness (18). Neither *GJB2* nor the Na<sup>+</sup>,K<sup>+</sup>-ATPase gene, however, appears to be a target of *Brn-4*-mediated regulation, because *Brn-4*-deficient fibrocytes showed no dramatic changes in the expression of either gene. Identification of *Brn-4* target genes in cochlear fibrocytes may help to elucidate the role of these cells in auditory function.

References and Notes

1. W. E. Nance et al., *Birth Defects* 7, 64 (1971); C. W. Cremers et al., *Arch. Otolaryngol.* 111, 249 (1985).
2. Y. J. M. de Kok et al., *Science* 267, 685 (1995).
3. R. J. McEvilly et al., *Nature* 384, 574 (1996); L. Erkmann et al., *ibid.* 381, 603 (1996).
4. D. Phippard et al., *Hear. Res.* 120, 77 (1998).
5. A 1.3-kb Acc I-Bam HI fragment and a 6-kb Eco RI fragment isolated from a J1 genomic DNA library were used as short and long homologous sequences of a targeting vector, respectively. The pgk-neo cassette flanked by a pair of loxP sequences was used for positive selections, and the diphtheria toxin A-chain gene cassette without a polyadenylation site was used for negative selection. The Not I-linearized targeting vector was introduced into J1 ES cells derived from 129/sv mice by electroporation and cells were selected with G418 (17).
6. An OCTA26 probe (GATCAGTACTAATAGCAT-TATAAAG) was used.
7. Mice were anesthetized with sodium pentobarbital (70 mg/kg) and maintained in a headholder within an acoustically and electrically insulated test room. Needle electrodes were placed on the tympanic bulla (positive lead) and scalp vertex (negative lead). Acoustic stimuli

evoked by a click were delivered and the ABRs were measured with an evoked potential recording system (NEC, Tokyo). The peak amplitude was measured peak to trough and the threshold was defined as 1 μV.

8. Horizontal sections of the temporal bone showed no gross difference between wild-type and mutant mice in the thickness of the stapes footplate or in the size or shape of the bony labyrinth, including the internal auditory meatus.
9. Under deep anesthesia, cochleas from 11-week-old mice were fixed with 4% paraformaldehyde (PFA) in 0.1 M phosphate buffer (pH 7.4) overnight at 4°C. The specimens were decalcified with 0.12 M EDTA, dehydrated, and embedded in paraffin. Serial sections (6 μm) were stained with hematoxylin and eosin. Five sections containing the supratracheal zone of the midbasal turn were selected at random and the number of fibrocytes (mean ± SD) was counted in sections from wild-type (590 ± 25) (n = 4) and mutant (605 ± 50) (n = 4) male mice.
10. Mice at postnatal day 0 were anesthetized and perfused with ice-cold 4% PFA and immersed in 4% PFA at 4°C overnight. Heads were embedded in OCT compound (Sakura) and cryosectioned (20 μm). Digoxigenin-labeled RNA probes were synthesized by using a 390-base-pair fragment of the 3' noncoding region of mouse *Brn-4* as a template (Boehringer). Tissue sections were treated with 4% PFA, washed in phosphate-buffered saline, and then hybridized with the probes at 72°C for 24 hours. Sections were washed under stringent conditions and hybridization signals were detected by immunohistochemical analysis.
11. B. A. Schulte and J. C. Adams, *J. Histochem. Cytochem.* 37, 127 (1989); S. S. Spicer and B. A. Schulte, *Hear. Res.* 56, 53 (1991); T. Kikuchi, R. S. Kimura, D. L. Paul, J. C. Adams, *Anat. Embryol.* 191, 101 (1995); S. S. Spicer and B. A. Schulte, *Hear. Res.* 100, 80 (1996).
12. Mice were anesthetized and perfused with 2.5% glutaraldehyde in 0.1 M sodium cacodylate buffer (pH 7.4). Cochleas were fixed by perilymphatic perfusion with 2.5% glutaraldehyde overnight at 4°C and immersed in the same fixative for 2 more hours at room temperature. Electron microscopy was performed as in (19).

13. In both wild-type and mutant mice, all three cell types of the stria vascularis (marginal, intermediate, and basal cells) were identified and presented a normal appearance. There was no observable difference in the structure of intrastrial capillaries between wild-type and mutant mice. Myelinated axons from spiral ganglion cells to sensory hair cells were well preserved. At the bases of inner hair cells, the fine structure of the afferent nerve terminal synapses appeared to be normal in mutant mice.
14. For EP measurement, each mouse was artificially ventilated with a respirator through a tracheal cannula after deep anesthesia and muscular relaxation. Rectal temperature was maintained at 37°C and an electrocardiometer was monitored. A glass microelectrode filled with 150 mM KCl was inserted into the scala media of the basal turn through the lateral wall of the cochlea and the output was recorded with a high-impedance dual electrometer (WPI), New Haven, CT.
15. H. Davis, *Cold Spring Harbor Symp. Quant. Biol.* 30, 181 (1965); V. Honrubia and P. H. Ward, *J. Acoust. Soc. Am.* 46, 388 (1969).
16. K. B. Avraham, *Nature Med.* 4, 1238 (1998); C. Kubisch et al., *Cell* 96, 437 (1999); S. Yasunaga et al., *Nature Genet.* 21, 363 (1999).
17. J. R. Bermingham Jr. et al., *Genes Dev.* 10, 1751 (1996); S. Nakai et al., *ibid.* 9, 3109 (1995); M. D. Schonemann et al., *ibid.*, p. 3122.
18. D. P. Kelsell et al., *Nature* 387, 80 (1997); X. Estivill et al., *Lancet* 351, 394 (1998).
19. Y. Katori, C. M. Hackney, D. N. Furness, *Cell Tissue Res.* 284, 473 (1996).
20. Supported by a grant-in-aid for Scientific Research on Priority Areas (O.M., T.N.); grant-in-aid 07457394 (K.I.) from the Ministry of Education, Sports, Science and Culture of Japan; and a grant from the Ministry of Health and Welfare. We thank M. Ogawa, K. Kaga, and T. Murobushi for valuable discussions; K. Jishage, H. Nishino, R. Sato, and K. Yamaguchi for technical support; and T. Morizono, C. M. Hackney, and D. N. Furness for support.

17 February 1999; accepted 30 June 1999

## Long-Term Depression in Hippocampal Interneurons: Joint Requirement for Pre- and Postsynaptic Events

Fernanda Laezza,<sup>1,2</sup> James J. Doherty,<sup>2</sup> Raymond Dingledine<sup>2\*</sup>

Long-term depression (LTD) is a well-known form of synaptic plasticity of principal neurons in the mammalian brain. Whether such changes occur in interneurons is still controversial. CA3 hippocampal interneurons expressing Ca<sup>2+</sup>-permeable AMPA receptors exhibited LTD after tetanic stimulation of CA3 excitatory inputs. LTD was independent of NMDA receptors and required both Ca<sup>2+</sup> influx through postsynaptic AMPA receptors and activation of presynaptic mGluR7-like receptors. These results point to the capability of interneurons to undergo plastic changes of synaptic strength through joint activation of pre- and postsynaptic glutamate receptors.

LTD and long-term potentiation (LTP) are activity-dependent forms of synaptic plasticity that have been extensively studied in the

hippocampus, neocortex, and cerebellum (1, 2). Most studies related to LTD and LTP have examined excitatory synapses onto principal neurons. However, it is important to know whether the same types of long-term plasticity occur at excitatory synapses onto interneurons. It is clear that long-term plasticity at certain hippocampal interneurons is passive, resulting from plasticity of excitatory inputs

<sup>1</sup>Neuroscience Graduate Program, <sup>2</sup>Department of Pharmacology, Emory University School of Medicine, Atlanta, GA 30322, USA.

\*To whom correspondence should be addressed. E-mail: rdingledine@pharm.emory.edu